TP53 missense mutations in PDAC are associated with enhanced fibrosis and an immunosuppressive microenvironment

Martino Maddalena[a], Giuseppe Mallel[a], Nishanth Belugali Nataraj[b], Michal Shreberk-Shaked[a], Ori Hassin[a], Saptaparna Mukherjee[a], Sharathchandra Arandkar[a,c], Ron Rotkopf[d], Abby Kapsack[a], Giuseppina Lambiase[a], Bianca Pellegrino[a], Eyal Ben-Isaac[d], Ofra Golani[d], Yoseph Addadi[d], Emma Hajaj[e], Raya Eilam[f], Ravid Straussman[a], Yosef Yarden[b], Michal Lotem[e], and Moshe Oren[a,1]

[a]Department of Molecular Cell Biology, Weizmann Institute of Science, 76100 Rehovot, Israel; [b]Department of Biological Regulation, Weizmann Institute of Science, 76100 Rehovot, Israel; [c]Advanced Centre for Treatment, Research and Education in Cancer, Tata Memorial Centre, 410210 Kharghar, India; [d]Department of Life Sciences Core Facilities, Faculty of Biochemistry, Weizmann Institute of Science, 76100 Rehovot, Israel; [e]Sharett Institute of Oncology, Hadassah Hebrew University Hospital, 91120 Jerusalem, Israel; and [f]Department of Veterinary Resources, Weizmann Institute of Science, 76100 Rehovot, Israel

Contributed by Moshe Oren, April 29, 2021 (sent for review December 13, 2020; reviewed by David A. Tuveson and Karen H. Vousden)

Pancreatic ductal adenocarcinoma (PDAC) is a highly lethal cancer, which is refractory to all currently available treatments and bears dismal prognosis. About 70% of all PDAC cases harbor mutations in the *TP53* tumor suppressor gene. Many of those are missense mutations, resulting in abundant production of mutant p53 (mutp53) protein in the cancer cells. Analysis of human PDAC patient data from The Cancer Genome Atlas (TCGA) revealed a negative association between the presence of missense mutp53 and infiltration of $CD8^+$ T cells into the tumor. Moreover, $CD8^+$ T cell infiltration was negatively correlated with the expression of fibrosis-associated genes. Importantly, silencing of endogenous mutp53 in KPC cells, derived from mouse PDAC tumors driven by mutant Kras and mutp53, downregulated fibrosis and elevated $CD8^+$ T cell infiltration in the tumors arising upon orthotopic injection of these cells into the pancreas of syngeneic mice. Moreover, the tumors generated by mutp53-silenced KPC cells were markedly smaller than those elicited by mutp53-proficient control KPC cells. Altogether, our findings suggest that missense p53 mutations may contribute to worse PDAC prognosis by promoting a more vigorous fibrotic tumor microenvironment and impeding the ability of the immune system to eliminate the cancer cells.

p53 | PDAC | fibrosis | immune infiltration | tumor microenvironment

Pancreatic ductal adenocarcinoma (PDAC) is one of the most lethal human cancers. It is often diagnosed at advanced stages, when complete surgical removal is not possible anymore, and resistance is acquired to all currently available therapies. As a result, less than 10% of the patients diagnosed with PDAC survive more than 5 y. The introduction of immune checkpoint blockade therapy has revolutionized the treatment of several types of cancer, most notably melanoma, lung cancer, and microsatellite unstable colorectal cancer. Unfortunately, to date, the PDAC immunotherapy regimen, either alone or in combination, has not yielded promising results in patients with metastatic disease (1). The inefficacy of immunotherapy is likely to be due, at least in part, to the immunosuppressive nature of the PDAC tumor microenvironment (TME), which is characterized by highly desmoplastic stroma and immunosuppressive cell populations (2–4). In particular the extensive fibrosis, involving the pathological deposition of dense extracellular matrix (ECM) around the PDAC cancer cells, can provide a physical and chemical barrier that impairs lymphocyte infiltration, compromising the ability of cytotoxic T cells to engage and eliminate the cancer cells (5–10).

Activated pancreatic stellate cells, commonly referred as cancer associated fibroblasts (CAFs), are a major component of the pancreatic TME. CAFs can act in multiple ways to promote tumor growth and metastasis (11, 12). Of note, PDAC CAFs can sequester $CD8^+$ T cells and reduce their infiltration into the peritumoral compartment of the tumor (6), while antifibrotic treatment disrupts stromal barriers and modulates the immune landscape, improving pancreatic cancer response to immune checkpoint blockade (13, 14).

The p53 protein, encoded by the *TP53* gene, is a tumor suppressive transcription factor that serves as a major barrier against the emergence and progression of many types of cancer (15). The *TP53* gene is mutated in about half of all human cancer cases. Unlike other tumor suppressor genes, the mutational landscape of *TP53* is dominated by missense mutations, which are often associated with enhanced stabilization and accumulation of mutant p53 (mutp53) protein within the cancer cells. Numerous studies have revealed that at least some of the more common *TP53* mutations, and in particular the major hotspot mutations, not only abrogate p53's tumor-suppressive role, but also confer upon the mutp53 proteins new oncogenic gain-of-function (GOF) activities. Such GOF of mutp53 is believed to be due, at least in part, to its ability to engage in a variety of protein–protein interactions and thereby modulate the transcriptional landscape of the cell and also impact

Significance

Pancreatic ductal adenocarcinoma (PDAC) is a highly lethal cancer, which is presently refractory to all available therapeutic strategies. PDAC tumors are characterized by a high degree of fibrosis, believed to be a major contributor to their therapy resistance. Mutations in the*TP53* tumor suppressor gene are very frequent in PDAC. We now report that *TP53* missense mutations, which lead to production of mutant p53 proteins, increase the extent of fibrosis and reduce the infiltration of cytotoxic $CD8^+$ T cells. The inhibition of $CD8^+$ T cell infiltration may augment the ability of PDAC tumors to evade the immune system. Hence, inhibition of the activities of mutant p53 may potentially sensitize PDAC tumors to anticancer treatments, including immunotherapy.

Author contributions: M.M. and M.O. designed research; M.M., N.B.N., O.H., S.M., and E.H. performed research; A.K., G.L., and B.P. helped with experiments; R.S. and Y.Y. supervised experiments; Y.A. and R.E. contributed new reagents/analytic tools; M.M., G.M., M.S.-S., S.A., R.R., E.B.-I., and O.G. analyzed data; and M.M., M.L., and M.O. wrote the paper.

Reviewers: D.A.T., Cold Spring Harbor Laboratory; and K.H.V., Francis Crick Institute.

The authors declare no competing interest.

[1]To whom correspondence may be addressed. Email: moshe.oren@weizmann.ac.il.

This article contains supporting information online at https://www.pnas.org/lookup/suppl/doi:10.1073/pnas.2025631118/-/DCSupplemental.

Published June 4, 2021.

directly a variety of cellular processes (16, 17). Of note, about 70% of all PDAC tumors harbor *TP53* gene mutations (18).

Perturbation of p53 in cancer cells can affect ECM deposition and stromal modification (19–21). Alterations in p53 in pancreatic cancer cells were shown to trigger cell-extrinsic effects and influence the features of surrounding stromal CAFs (22). Importantly, the p53 status of the cancer cells can impact in many ways the tumor immune microenvironment and the interaction of the immune system with the cancer cells (reviewed in ref. 23). For example, wild-type (WT) and mutant variants of p53 can modulate in diverse manners the antigen presentation machinery and regulate the expression of activating ligands for NK cells and of immunosuppressive molecules such as PDL1. Moreover, p53 status can influence cytokine and chemokine secretion from the cancer cells, thereby greatly impacting the immune TME (23–25). Likewise, cancer cells expressing GOF mutp53 can reprogram macrophages through exosome-based communication (26), and loss of function of p53 can trigger cancer-protective systemic inflammation (25) and attenuate T cell activation by triggering a suppressive myeloid response (27). Notably, correlations between p53 status and immune infiltration have been observed in breast, head-and-neck, and gastric cancers (28, 29).

In the present study, we set out to elucidate the impact of missense *TP53* mutations on the immune TME of PDAC. Based on the analysis of TCGA data, human tumor samples and orthotopic mouse PDAC xenografts, we now report that the presence of missense mutp53 restricts the infiltration of cytotoxic $CD8^+$ T cells into PDAC tumors. This is associated with, and may be partly due to, elevated expression of ECM-related genes and increased fibrosis. Interference with mutp53-dependent processes may thus facilitate the application of immunotherapy to PDAC tumors.

Results

***TP53* Missense Mutations Are Associated with Short-Term Survival of PDAC Patients.** To explore the impact of p53 mutations in PDAC, TCGA PDAC samples (adenocarcinoma histological type) were divided into WT p53 tumors, p53-null tumors (harboring frameshift and nonsense mutations), and tumors with *TP53* missense mutations.

Mutp53 GOF is believed to be driven by elevated steady-state levels of mutp53 proteins, largely owing to their extensive stabilization. In agreement, examination of reverse phase protein array (RPPA) data in TCGA confirmed the presence of significantly higher amounts of p53 protein in PDAC tumors harboring p53 missense mutations, relative to wtp53 tumors (Fig. 1*A*). As expected, tumors with null mutations had the lowest p53 protein levels, even though some of them may still express residual truncated p53. Two p53 missense mutated tumors displayed p53 levels lower than the median of the p53-null tumors, and thus were excluded from further analyses. Altogether, we ended up with 48 WT p53 tumors, 31 p53-null tumors, and 31 tumors harboring missense *TP53* mutations.

To assess the impact of p53 mutational status on overall patient survival, we compared the percentage of short-term survivors (STSs; overall survival <1 y after initial diagnosis), long-term survivors (LTSs; overall survival >3 y after initial diagnosis), and middle-term survivors (MTSs; overall survival 1 to 3 y after initial diagnosis) in the different p53 status groups. Of note, the vast majority of these tumors were derived from patients diagnosed at an early stage of the disease (30), when tumor resection is still applicable, accounting for the relatively long overall survival. Remarkably, whereas in the null and WT p53 groups about 20% of patients attained long-term survival, only 5% of missense mutated patients survived for longer than 3 y (Fig. 1 *B–D*).

These observations suggest that the presence of p53 missense mutations in PDAC patients is associated with worse disease outcome than in p53 null and WT p53 cases. In particular, the comparison with the p53-null tumors supports the notion that p53 missense mutants possess an oncogenic GOF in PDAC.

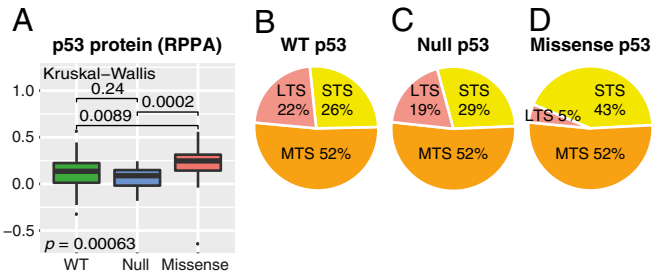

Fig. 1. p53 missense mutations in PDAC are associated with elevated p53 protein levels and shorter survival. PDAC samples from TCGA (PAAD dataset filtered by adenocarcinoma histological type) were divided into WT p53, p53-null (frameshift and nonsense *TP53* mutations), and p53 missense mutated tumors. (*A*) Relative levels of p53 protein in each group, as determined by RPPA data in TCGA. (*B–D*) Percentage of short-term survivors (STSs; overall survival <1 y after initial diagnosis), middle-term survivors (MTSs; overall survival 1 to 3 y after initial diagnosis), and long-term survivors (LTSs; overall survival >3 y after initial diagnosis) within each group of PDAC patients.

Human PDAC Tumors Harboring *TP53* Missense Mutations Display Reduced $CD8^+$ T Cell Infiltration. The abundance and composition of tumor-infiltrating immune cells can affect cancer progression and response to therapy (31). Hence, we assessed the relationship between p53 mutational status and the tumor-associated immune cell composition in PDAC. The composition of distinct stromal cell populations can be estimated from bulk tumor gene expression data, taking advantage of distinctive gene signatures characteristic of each population. Remarkably, comparison of the Knudsen et al. (32) lymphocyte gene signatures between p53 missense, null, and WT PDAC tumors in TCGA revealed that cases with missense p53 mutations were preferentially enriched among the tumors that displayed low lymphocyte signatures, relative to p53-null and WT cases (Fig. 2*A*). Interestingly, some of the WT p53 tumors displayed high numbers of $CD8^+$ T cells but relatively low numbers of $CD4^+$ regulatory T cells (Tregs), consistent with a recent report by Blagih et al. (27). We then aggregated the signatures of the different lymphocyte subpopulations from Knudsen et al. (32) (displayed in Fig. 2*A*) into a single lymphocyte signature and ranked all tumors accordingly (*SI Appendix*, Fig. S1). Comparison of the top quartile (highest lymphocyte signature) and bottom quartile (lowest lymphocyte signature) (*SI Appendix*, Fig. S1) further confirmed that tumors displaying a low lymphocyte score are enriched with missense *TP53* mutations (Fig. 2*B*). Importantly, patients with a low lymphocyte signature tend to have a shorter survival than those with a higher signature (Fig. 2*C*). A similar correlation between p53 missense mutations and reduced numbers of tumor-infiltrating lymphocytes was seen when we applied the Thorsson et al. (33) lymphocyte infiltration score to the same PDAC dataset (Fig. 2*D*).

Importantly, comparative analysis of the PDAC immune landscape, as described in Thorsson et al. (33), identified $CD8^+$ T cells as the population most significantly associated with differences in p53 mutational status (Fig. 2*E*), when compared to other types of lymphocytes or to myeloid cells (*SI Appendix*, Fig. S2*A*). Likewise, application of the gene signature of Puram et al. (34) confirmed that missense mutated tumors are characterized by a significantly reduced abundance of $CD8^+$ cytotoxic cells (*SI Appendix*, Fig. S2*B*).

To further investigate the correlation between the presence of missense mutp53 and the paucity of $CD8^+$ T cells in PDAC, we analyzed two tissue microarrays (TMAs) of human PDAC tumors comprising a total of 83 informative samples. Strong positive staining for p53 is generally considered indicative of the presence of GOF

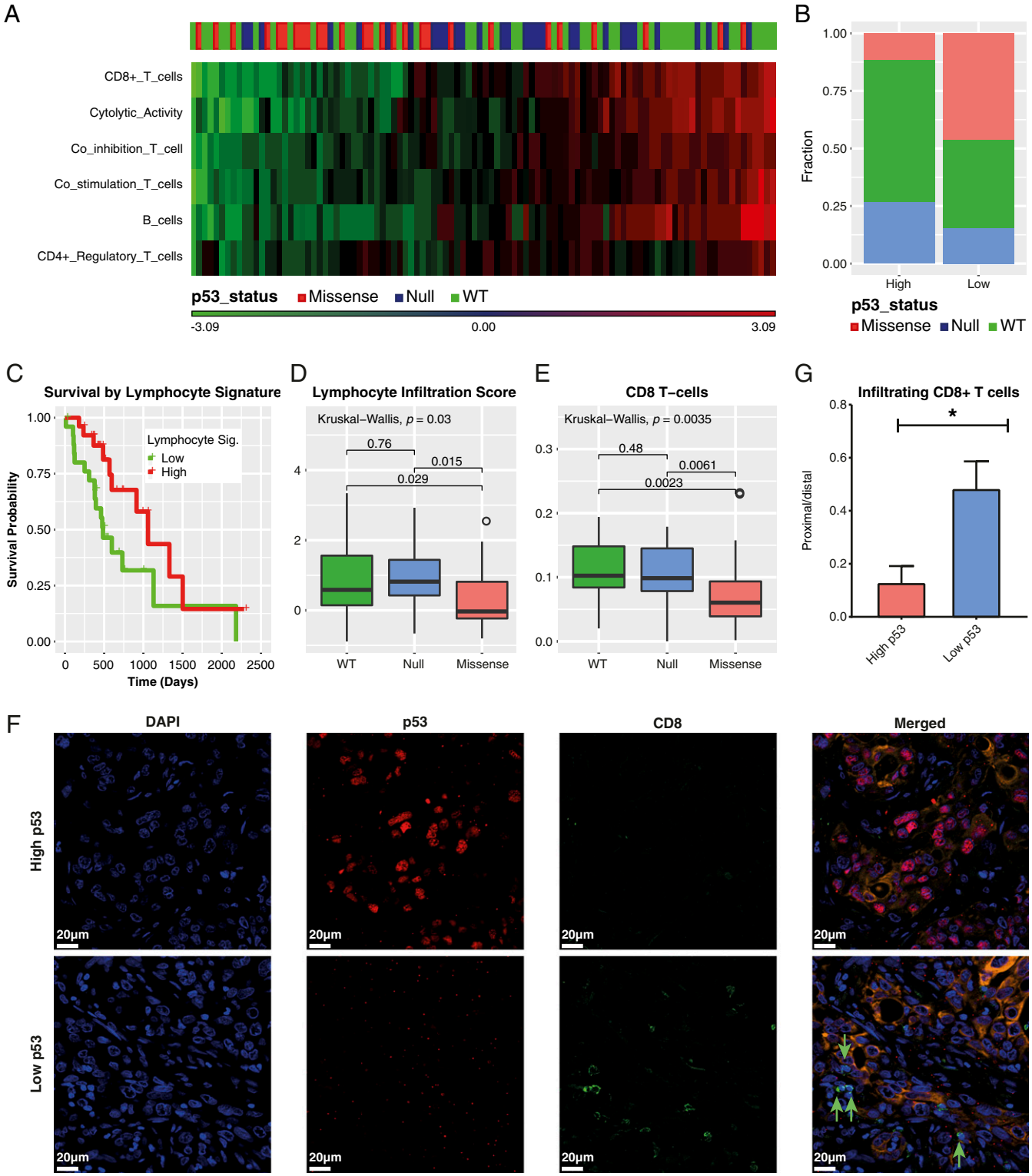

Fig. 2. PDAC tumors harboring p53 missense mutations display reduced lymphocyte infiltration. (*A*) Heat map depicting the relative abundance of various classes of infiltrating lymphocytes in TCGA PDAC tumors. Each vertical column represents a single tumor. The relative abundance of the indicated lymphocyte classes in each tumor was deduced from their distinctive gene expression signatures, as described in Knudsen et al. (32). The p53 status of each tumor is noted on *Top*. (*B*) Tumors in *A* were ranked according to the strength of their lymphocyte signature, calculated by aggregating all lymphocyte subpopulation signatures in *A*. The fractions of WT, null, and missense p53 mutated cases within the top quartile (highest lymphocyte signature) and bottom quartile (lowest lymphocyte signature) are shown. (*C*) Kaplan–Meier survival plot comparing cases with high vs. low aggregated lymphocyte signature as in *B*; *P* value = 0.037. (*D*) Lymphocyte infiltration signature score, calculated according to Thorsson et al. (33), in the different p53 status groups. (*E*) Estimated relative abundance of $CD8^+$ T cells calculated according to Thorsson et al. (33), in the different p53 status groups. (*F*) Representative examples of p53, CK8, and CD8 staining in tumor samples from a PDAC tissue microarray. $CD8^+$ T cells are marked with green arrows in the merged picture. (*G*) Relative spatial distribution of infiltrating $CD8^+$ T cells in low p53 vs. high p53 PDAC tumors. See *Materials and Methods* for further details. Values represent means ± SEM; *P* value: $^*P < 0.05$.

missense p53 mutations, owing to stabilization of the mutp53 protein. We therefore employed intense p53 staining as a proxy for identification of TMA samples harboring GOF mutp53. In parallel, the same set of tumor samples was stained for CD8, as well as for CK8 to highlight epithelial cells (Fig. 2*F*). Altogether, 13 tumors showed high nuclear p53 staining (intense staining in more than 15% of the cancer cells), whereas the other 70 tumors had no, or only weak, staining, suggesting that they might have retained WT *TP53*, or may carry frameshift or nonsense *TP53* mutations, or express nonstabilized missense mutp53. For each tumor sample, we then analyzed the spatial distribution of $CD8^+$ T cells in six nonoverlapping fields. We counted for each field the number of proximal $CD8^+$ T cells (located either within epithelial cancer cell clusters or less than 10 μm from the nearest cancer cell), and distal $CD8^+$ cells (located more than 10 μm from the nearest cancer cell) (*SI Appendix*, Table S1). After normalization for the percentage of epithelial cancer cells and of stroma in each field (*Materials and Methods*), we calculated for each individual sample the ratio between the number of proximal versus distal $CD8^+$ cells. As seen in Fig. 2*G*, this analysis revealed that in tumors displaying high p53 staining, $CD8^+$ T cells tended to stay further away from the cancer cells than in low p53 tumors. This further supports the conjecture that mutp53 may hamper the infiltration of cytotoxic T cells within PDAC tumors.

Together, our observations suggest that the presence of missense mutp53 may disfavor the infiltration of lymphocytes, particularly cytotoxic $CD8^+$ T cells, into PDAC tumors, possibly leading to worse patient outcome. The fact that such effect is not seen in p53-null tumors strongly argues that this may constitute a GOF activity of mutp53.

Mutant p53 Restricts $CD8^+$ T Cell Infiltration and Promotes Tumor Growth in an Orthotopic Mouse PDAC Model. To assess more directly the impact of p53 missense mutations on $CD8^+$ T cell infiltration in PDAC, we silenced the endogenous mutp53 in two independent cell lines (KPC-3 and KPC-4), derived from PDAC tumors of KPC (LSL-KrasG12D/+; LSL-Trp53R172H/+; Pdx-1-Cre) mice (kind gift from D. Tuveson, Cold Spring Harbor Laboratory, New York). In KPC mice, mutant Kras and the p53R172H mutant, equivalent to the R175H human hotspot p53 mutant, are specifically expressed in the pancreas, giving rise to aggressive PDAC tumors (35). Control KPC-3 cells (shC) and their mutp53-knockdown derivatives (shp53) were injected orthotopically into the pancreata of syngeneic C57/BL6 mice, and tumors were harvested 2 wk later. Analysis by immunohistochemistry revealed that the KPC-3 shC tumors, which express abundant mutp53, had markedly less infiltration of $CD8^+$ T cells compared to the mutp53-depleted shp53 cells (Fig. 3 *A* and *B*). Similar results were obtained in a second KPC cell line (KPC-4), derived from a different mouse (*SI Appendix*, Fig. S3*A*).

Reduced infiltration of cytotoxic T cells is expected to facilitate tumor immune evasion, possibly accelerating tumor growth. As seen in Fig. 3 *C* and *D*, shC tumors, retaining expression of endogenous mutp53, gave rise to bigger tumors than mutp53-depleted cells when injected orthotopically into syngeneic mice. Importantly, the effect of mutp53 on tumor growth was markedly less pronounced in immunodeficient mice (both athymic nude and NSG; Fig. 3*E*), as confirmed also for another independently derived PDAC cell line (KPC-4; see *SI Appendix*, Fig. S3*B*).

Altogether, these observations support the conjecture that mutp53 contributes to enhanced PDAC tumor growth by suppressing the infiltration of cytotoxic effector cells, although T cell-independent effects of mutp53 also could play a role in promoting tumor growth. The above findings establish a causal relationship between the presence of stabilized missense mutp53 and reduced infiltration of $CD8^+$ T cells and imply that mutp53 may exert an oncogenic GOF in PDAC by favoring tumor immune evasion.

p53 Missense Mutations in PDAC Are Associated with Increased Fibrosis. To point out putative mutp53-dependent mechanisms underpinning the inhibition of $CD8^+$ T cell infiltration in PDAC, we employed the TCGA PDAC cohort to infer genes whose expression is correlated positively and negatively, respectively, with the $CD8^+$ T cell signature indicated in Fig. 2*E*. The result of this analysis is shown in Fig. 4*A*. As expected, CD8A, GZMB, and PRF1, indicative of cytotoxic $CD8^+$ T cells, ranked high among the positively correlated genes. Interestingly, functional profiling in g:Profiler (36) of the genes negatively correlated with the $CD8^+$ T cell signature (Fig. 4*B*) revealed enrichment for proteins residing in extracellular space (GO:CC) and for functional terms related to fibrosis, such as Rho GTPase signaling, ECM organization, and collagen formation (REAC). This supports the notion that excessive desmoplastic response hinders the ability of immune cells to infiltrate PDAC tumors (13, 14, 37, 38).

We then compared the relative expression levels of two of the functional signatures in Fig. 4*B* (collagen formation and extracellular matrix organization) among human PDAC tumors of different *TP53* status. Remarkably, expression of those fibrosis-associated genes was significantly up-regulated in missense mup53 tumors, compared to p53-null and WT tumors (Fig. 4 *C* and *D*). This observation is consistent with a recent report by Vennin et al., who found that GOF mutp53 can increase fibrosis in KPC tumors (22).

Tian et al. (39) have recently defined a set of cancer cell ECM proteins ("matrisome") associated with poor survival in PDAC. CAFs are the major source of ECM proteins, and stromal cells produce over 90% of the total ECM mass of PDAC tumors. Nevertheless, Tian et al. found that elevated levels of ECM and ECM-associated proteins produced by the cancer cells ("cancer matrisome"), and not those produced exclusively by PDAC stromal cells, correlate strongly with poor patient survival (39). Using the gene signatures developed by Tian et al., we interrogated the relative representation of the cancer matrisome genes associated with poor survival in the three *TP53* status groups in TCGA. Remarkably, this analysis revealed a significant association between p53 missense mutations and elevated expression of genes comprised in the PDAC poor survival matrisome, relative to p53-null tumors (Fig. 4*E*). Furthermore, the PDAC poor survival matrisome gene signature displayed a significant negative correlation with the estimated $CD8^+$ T cell content (Fig. 4*F*).

Together, these observations imply an association between missense mutp53 and altered composition of the PDAC ECM, which might lead to reduced infiltration of cytotoxic T cells and possibly contribute to poor patient survival.

Missense p53-Dependent Fibrosis Is Negatively Correlated with $CD8^+$ T Cell Infiltration in KPC Orthotopic Tumors and Human PDAC. To corroborate the correlation between high fibrosis and low $CD8^+$ T cell infiltration, orthotopically injected KPC-3 tumors were stained with Sirius Red to visualize collagen fibers. Indeed, shC tumors showed more fibrosis than shp53 tumors (Fig. 5 *A* and *B*), as observed also in tumors derived from a different KPC cell line (KPC-4, see *SI Appendix*, Fig. S4*A*). Hence, mutp53 promotes fibrosis in this syngeneic PDAC model. This is consistent with a previous report of increased fibrillar collagen density in matrices remodeled by CAFs educated by mutp53-proficient KPC cells, as compared to those educated by mutp53-deficient ones (22) Importantly, the extent of $CD8^+$ T cell infiltration was inversely proportional to Sirius Red staining (Fig. 5*C* and *SI Appendix*, Fig. S4*B*).

To explore the relationship between p53 status, collagen deposition and $CD8^+$ T cell infiltration in human PDAC, we imaged fibrillar collagen by second harmonic generation (SHG) microscopy, which allows imaging of noncentrosymmetric molecules such as collagen fibers. We analyzed the collagen deposition within 10 μm from the cancer cells in tumors with high p53 staining versus tumors with low p53 staining. Indeed, in tumors

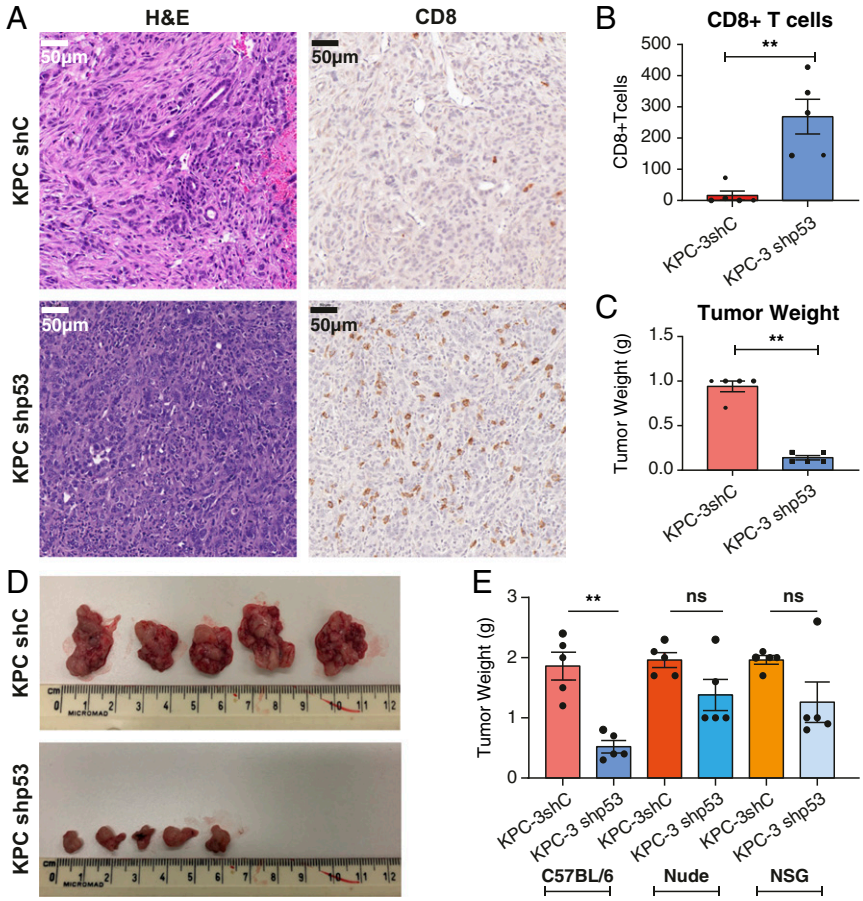

Fig. 3. Depletion of endogenous mutp53 augments CD8$^+$ T cell infiltration and favors tumor growth in an orthotopic mouse PDAC model. (*A*) Mouse KPC-3 PDAC cells, expressing endogenous mutp53 R172H, were stably transduced by infection with recombinant lentiviruses expressing either mouse p53 shRNA (shp53) or control shRNA (shC). A total of 20,000 cells of each genotype were injected orthotopically into the pancreata of C57BL/6 mice (eight mice per group). Tumors were harvested after 2 wk and tumor sections were stained for CD8. Representative tumor sections (20× magnification) are shown. (*B*) Quantification of CD8$^+$ T cells based on five tumors from each genotype in *A*. For each tumor, CD8$^+$ cells were counted in three images taken at 20× magnification. Mean ± SEM for each tumor group is shown. *P* value: $^{**}P < 0.01$. (*C*) Quantification of tumor weight, based on five tumors from each genotype in *A*, harvested 2 wk after orthotopic injection. Mean + SEM. *P* value: $^{**}P < 0.01$. (*D*) Photographs of the same tumors as in *C*. (*E*) Comparison of tumor weight in syngeneic versus immunodeficient mice. KPC-3 cells were injected orthotopically in parallel into the pancreata of C57BL/6, NSG, and athymic nude mice, as in *A*. To attain comparable sizes of shC tumors in all three genotypes, syngeneic C57BL/6 mice were killed 4 wk after injection, whereas immunocompromised mice were killed after 3 wk. Mean ± SEM. *P* value: $^{**}P < 0.01$; ns, not significant.

staining strongly for p53, the percentage of the tumor area occupied by stromal collagen was significantly higher than in those staining weakly for p53 (Fig. 5 *D* and *E*).

Together, our observations imply that p53 missense mutations impair the infiltration of cytotoxic CD8$^+$ T cells into PDAC tumors, and this may be due at least in part to the enhancement of fibrosis.

Discussion

Immune evasion, fibrosis, and modulation of the tumor microenvironment have emerged as important features of PDAC pathology and determinants of clinical outcome (40–42). Yet, the molecular and genetic mechanisms that shape cancer and stroma cell heterogeneity and that are responsible for their variation among individual patients remain to be fully elucidated. Furthermore, human PDAC tumors are typically "cold," displaying very low levels of tumor infiltrating T cells, most probably accounting for the poor efficacy of immune therapy in this type of cancer (43). Consequently, attempts are being made to convert the "immune cold" PDAC microenvironment into a more inflamed TME, with the hope that increased T cell infiltration and activity will sensitize these tumors to cancer immunotherapy (44).

In the present study, we report that the presence of *TP53* missense mutations can selectively reduce CD8$^+$ T cell infiltration in PDAC tumors, in correlation with the ability of missense mutp53 to augment ECM deposition. Desmoplastic reaction, involving enhanced CAF activation and ECM deposition and remodeling, plays an important role in tumor progression, resistance to therapy, and immunomodulation in multiple cancer types. In particular, stromal content, matrix architecture, and collagen density can dictate the localization and activity of tumor-infiltrating T cells and the ability of CD8$^+$ T cells to target effectively the cancer cells within the tumor (6, 40–44).

Despite the well-documented role of the desmoplastic response in PDAC, targeting the pancreatic TME as a means for achieving better therapeutic outcome has yielded inconsistent conclusions and needs to be further explored. On the one hand, depletion of FAP$^+$ stromal cells in a murine PDAC model facilitated immune control of tumor growth and uncovered the efficacy of anti-PD-L1 immunotherapy (5). Likewise, inhibition of FAK activation, thereby curtailing a major mechanism of ECM-driven signaling, was shown to reduce fibrosis, increase the amount of cytotoxic T cells, and significantly hinder tumor progression (14). On the other hand, depletion of α-smooth muscle actin (α-SMA)-positive CAFs resulted in

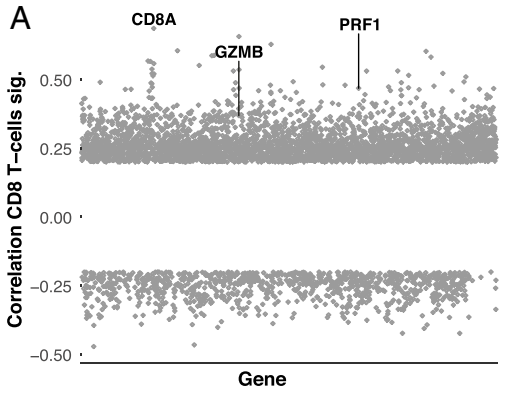

B

Source	Term_name	Adjusted_p_value	Term_size	Query_size	Intersection_size
GO:CC	focal adhesion	8.44E-04	430	868	44
GO:CC	cell-substrate junction	1.14E-03	428	473	50
GO:CC	extracellular space	4.99E-02	432	877	45
GO:CC	anchoring junction	7.09E+00	434	868	42
REAC	Signaling by Rho GTPases	2.14E+05	1591	895	111
GO:CC	cell junction	0.00001	583	823	56
GO:CC	supramolecular fiber	0.00001	633	600	100
GO:BP	cell-substrate adhesion	0.00023	119	868	22
REAC	Cell junction organization	0.00028	1902	868	185
GO:BP	hemidesmosome assembly	0.00093	134	823	22
REAC	Extracellular matrix organization	0.00246	2149	868	161
REAC	Collagen formation	0.00394	2242	877	175
GO:BP	supramolecular fiber organization	0.01050	232	868	28
GO:BP	cell-matrix adhesion	0.01957	291	877	30
GO:BP	regulation of cell-matrix adhesion	0.02149	300	868	35
GO:CC	cell-cell junction	0.02255	995	895	86

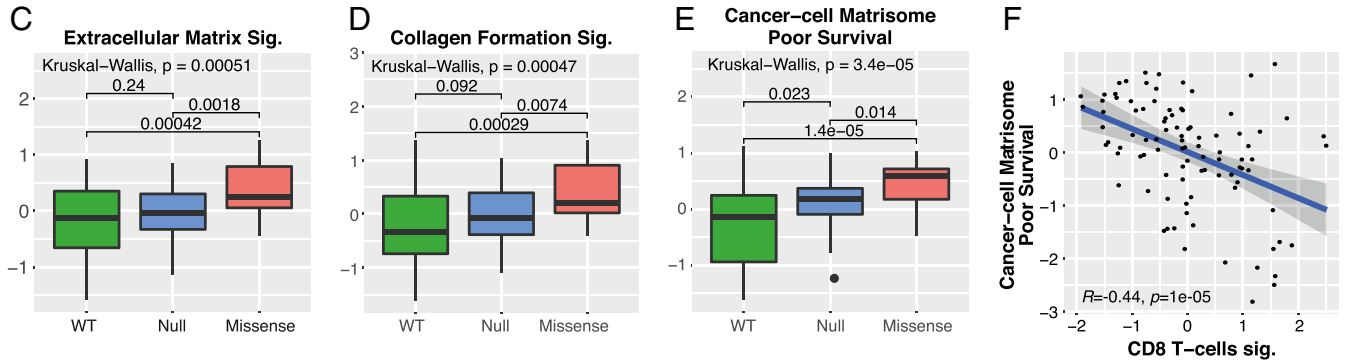

Fig. 4. p53 missense mutations in PDAC are associated with more fibrosis, which is negatively correlated with CD8$^+$ T cell infiltration. (*A*) Genes positively or negatively correlated with the CD8$^+$ T cell signature (Fig. 2*E*) in the TCGA PDAC cohort were defined by a cutoff of $R = 0.2$ or -0.2, respectively. The detailed gene list is provided in Dataset S1. (*B*) Functional profiling (g:Profiler) of genes negatively correlated with the CD8$^+$ T cell signature in *A*. g:Profiler output is provided in Dataset S2. (*C*) Relative expression of extracellular matrix signature genes in the three *TP53* status groups in TCGA. (*D*) Relative expression of collagen formation signature genes in the three *TP53* status groups in TCGA. (*E*) Relative expression of the PDAC cancer cell matrisome gene signature associated with poor survival (39) in the three *TP53* status groups in TCGA. (*F*) Correlation between the PDAC cancer cell matrisome gene signature associated with poor survival (39) and the estimated CD8$^+$ T cell abundance (Fig. 2*E*) in the TCGA PDAC cohort.

immunosuppression and aggressive tumors (45). Moreover, a clinical trial based on the use of a sonic hedgehog (SHH) pathway inhibitor, to reduce the PDAC stromal component, did not increase the efficacy of gemcitabine in human PDAC patients (46). Likewise, reduction of the stromal content in a mouse PDAC model by targeting the SHH pathway genetically, or by chronically inhibiting it, increased cancer aggressiveness (47). Therefore, full understanding of the determinants and mechanisms underlying stromal modulation and immunosuppression in PDAC may pave the road to more rational therapeutic strategies.

TP53 mutations are very frequent in PDAC, being second only to KRAS mutations. However, unlike in the case of KRAS, *TP53* mutations come in very different flavors and may have very different effects. In particular, while all cancer-relevant *TP53* mutations most probably abolish the tumor suppressive effects of WT p53, only missense but not null mutations may potentially confer GOF activities, and even this is very much context dependent (48–50). As seen in Fig. 1*B*, the presence of *TP53* missense mutations in PDAC is associated with worse patient prognosis. This apparent GOF effect of mutp53 is likely to be exerted via multiple molecular mechanisms. For example, mutp53 can promote PDAC metastatic propensity by elevating the expression of platelet-derived growth factor receptor b (PDGFRb), which is achieved through the ability of mutp53 to bind and inhibit the p53-related p73 protein (51). Furthermore, missense mutp53 in PDAC cancer cells can contribute to the formation of a prometastatic environment by increasing the production of ECM proteins (22), as also observed by us. This is in tune with similar studies in other cancer types, which demonstrated that mutp53, at least in part via cooperation with HIF1-alpha, can augment ECM deposition, thereby supporting stromal stiffening and promoting tumor growth and metastasis (20, 21).

As shown here, missense mutp53 can also restrict the infiltration of cytotoxic T cells into PDAC tumors, implicating anticancer immunity as an additional mechanism that is manipulated by GOF mutp53 in favor of tumor progression.

Notably, while p53 is usually not mutated in the tumor stroma, there is evidence that the WT p53 protein of stromal fibroblasts can be rewired in the course of tumor progression and contribute to the cancer-supportive features of the CAFs (52). It remains to be determined whether this applies also to PDAC CAFs, and whether missense mutp53 in the PDAC cancer cells may play an active role in the reconditioning of stromal WT p53, for example, by regulating exosome abundance and content (26, 53). Interestingly, p53 represses the expression of CXCL12/SDF1 in both human and mouse fibroblasts (52), and inactivation of p53 leads to augmented CXCL12 expression and secretion and increases the ability of the fibroblasts to support tumor growth (54). In that regard, it is notable that depletion, or inhibition, of CAF-derived CXCL12 sensitizes PDAC tumors to checkpoint blockade immunotherapy (5). Furthermore, a study that looked at multiple cancer types has revealed that tumors characterized by a high rate of *TP53* mutations tend to have a distinctive CAF ECM signature, often driven by TGF-beta, which is correlated with an immunosuppressive TME (55).

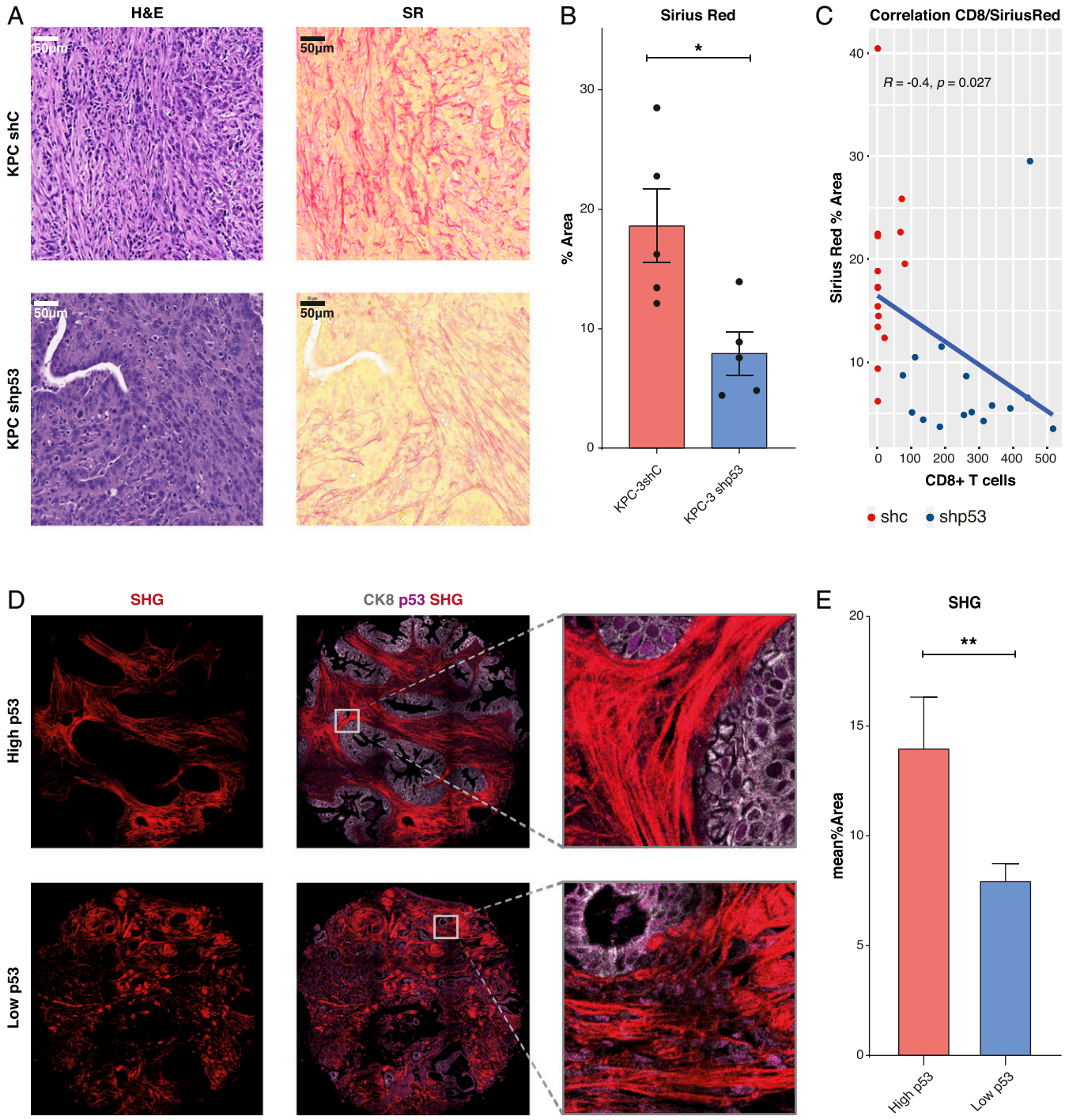

Fig. 5. Missense p53-associated fibrosis is negatively correlated with CD8$^+$ T cell infiltration in orthotopic mouse tumors and human PDAC patients. (*A*) Representative images of H&E- and Sirius Red-stained sections of tumors derived by injection of KPC-3 shC or shp53 cells into the pancreata of syngeneic C57BL/6 mice, as described in Fig. 3*A* (20× magnification). (*B*) Quantification of Sirius Red staining in KPC-3 shC and shp53 tumors. The percentage of tumor area occupied by collagen was calculated from five tumors of each genotype, by averaging the values obtained in three images per tumor taken at 20× magnification. *P* value: **P* < 0.05. (*C*) Correlation between % area occupied by collagen, determined in *B*, and number of CD8$^+$ cells calculated as in Fig. 3*B*. Each dot represents an image, together comprising 15 images from five mice of each genotype. (*D*) Representative images of collagen fibers, visualized by a SHG microscope, from a tumor with low p53 staining and a tumor with high p53 staining, respectively, in a human PDAC TMA. Images were taken at 40× magnification. (*E*) Quantification of collagen fibers in human samples, determined by SHG. Data from two TMAs were combined. Shown is the comparison of fraction area of positive collagen signal within 10-μm bands from neoplastic ducts in tumors with high p53 and low p53 staining (*Materials and Methods*). Means ± SEM; *P* value: ***P* < 0.01.

Augmented ECM deposition is not the only means whereby mutp53 keeps cytotoxic immune cells away from the cancer cells. In particular, while this paper was under revision, mutp53 was reported to inhibit immune cell infiltration by interacting with TANK binding protein kinase 1 (TBK1) and blunting the cGAS/STING pathway (56). Hence, mutp53 enlists multiple mechanisms

to facilitate tumor immune evasion. It is thus tempting to speculate that GOF missense p53 mutants may contribute to the inefficacy of checkpoint blockade therapy in PDAC, and that depletion of mutp53 (e.g., by targeted degradation) (57), or attenuation of its GOF effects, may sensitize PDAC tumors to such therapy. Further studies are required in order to assess the practicality and efficacy of such approaches and their potential impact on PDAC patient outcome.

Materials and Methods

Data Acquisition and Processing. TCGA RNA-sequencing (RNA-Seq) expression profiles, gene somatic mutations, protein expression profiles, and clinical data were downloaded from https://gdac.broadinstitute.org/ and xena.ucsc.edu/. TCGA PAAD (pancreatic adenocarcinoma) samples were filtered by adenocarcinoma histological type and divided according to their *TP53* status into WT p53 tumors, null tumors (harboring frameshift or nonsense mutations), and missense mutated tumors. TCGA-HV-A5A6-01A frameshift variant p.R342Efs*3 was excluded from the null list because the mutation is relatively close to the end of the protein and the possible functional impact of the resultant truncated protein is thus uncertain. Two p53 missense mutated tumors possessing p53 protein levels lower than the median of the null tumors, as determined by RPPA, were also excluded from the analysis, since they are not expected to have mutp53 GOF. Altogether, the samples included in the analysis comprised 48 WT, 31 null, and 31 missense p53 tumors.

Cell Lines and Cell Culture. KPC cell lines (generous gift from D. Tuveson) were derived from PDAC tumors arising in KPC mice on a C57BL/6 genetic background. These mice (Kras +/LSL-G12D; p53 +/LSL-R172H; PDX-Cre) express mutant Kras and mutp53 exclusively in their pancreata (58). In the present study we used two KPC cell lines, each derived from a separate mouse: KPC mT3-2D and KPC mT4-2D (abbreviated as KPC-3 and KPC-4, respectively). The cells employed in Fig. 3 also expressed GFP, whereas the cells in *SI Appendix*, Fig. S3 expressed GFP plus firefly luciferase.

All cells were maintained at 37 °C in a 5% (Vol/Vol) CO_2 humidified incubator and were regularly tested for mycoplasma. KPC cells and HEK293 Phoenix cells were cultured in DMEM (Dulbecco's Modified Eagle Medium, Biological Industries) supplemented with 10% fetal bovine serum (FBS) and 1% penicillin and streptomycin (P/S) (Biological Industries).

Viral Infections. KPC-3 cells were infected with recombinant lentiviruses based on the LMP-p53.1224 plasmid to knock down the endogenous mouse p53 (DOI: https://doi.org/10.1038/ng1651) (generous gift from V. Krizhanovsky, Weizmann Instute of Science) or LMP empty vector plasmid as control (shp53 and shc, respectively). KPC-4 cells were infected with recombinant lentiviruses based on plasmid TRCN0000012361 (Horizon/Dharmacon) to knock down mouse p53, or SHC002 pLKO1 (Sigma) as control (shp53 and shc, respectively). Lentiviral packaging was performed by jetPEI-mediated transfection of Phoenix cells with the indicated plasmid DNAs, together with a plasmid encoding the VSVG envelope protein. Virus-containing supernatants were collected 24 h and 36 h after transfection, filtered, and supplemented with 4 μg/mL polybrene (Sigma). Puromycin selection was initiated 48 h after infection and continued for a week. Efficiency of p53 knockdown was verified by qRT-PCR and Western blot analysis. After the first round of infection described above, the KPC-4-derived cells were additionally infected with a recombinant lentivirus (Addgene #62511) expressing luciferase, derived from a retroviral construct (Addgene #25894) carrying G418 resistance, and infected cells were selected with G418.

In Vivo Orthotopic Injection Model. All animal experiments and methods were approved by the Weizmann Institutional Animal Care and Use Committee. Genetically modified cells were injected orthotopically into the pancreata of male 14-wk-old C57BL/6, NSG, or athymic nude mice (20,000 cells/mouse in 20 μL of Matrigel; 1:1 with DMEM) (12). Tumors were harvested 2 wk postinjection, unless indicated otherwise in the figure legend.

Tissue Microarray. Human pancreas cancer tissue array 12 cases/24 cores (PA242e) and advanced stage pancreas cancer tissue array 96 cases/192 cores (PA1921a) were purchased from US Biomax, Inc. Of those, a total of 83 cases (10 + 73, respectively) were deemed of sufficient quality to be informative and were therefore included in the analysis.

Immunohistochemistry and Histological Data Analysis. The 4-μm sections of 2.5% PFA (formalin-fixed) paraffin-embedded (FFPE) tissue specimens were deparaffinized in xylene and rehydrated through graded ethanol. Antigen retrieval was performed in citrate buffer (CA) or in Tris-ethylenediamine tetraacetic acid (EDTA) buffer (in a microwave, 10 min). Tissues were blocked in 20% normal horse serum blocking solution, followed by avidin/biotin blocking solution (Vector). Slides were subjected to staining with the following antibodies: mouse CD8 (eBioscience clone 4SM15), p53 (CM5; NCL-L-p53-CM5p; Leica Biosystems) and human CD8 (abcam ab17147), CK8 (Millipore MABT329). All antibodies were diluted in PBS containing 2% normal horse serum. Sections were incubated overnight at room temperature. For immunofluorescence, sections were incubated with a biotinylated secondary antibody, followed by conjugated streptavidin. Then, nuclei were counterstained with DAPI. For Diaminobenzidine (DAB) staining, a 30-min incubation in quenching solution (methanol, H_2O_2, HCl) was applied before antigen retrieval. After primary antibody incubation, biotinylated antibodies were applied followed by incubation in Avidin-Biotin Complex Staining Kits (ABC Kits). Hematoxylin was used for nuclear staining. Dehydration and incubation in xylene were performed before mounting.

Quantification of $CD8^+$ Cells. Stained mouse and human tissue samples were digitally scanned at high resolution and viewed using Aperio ImageScope. We identified mouse PDAC-positive areas within hematoxylin and eosin (H&E)-stained sections. Likewise, this approach was used to identify and exclude necrotic areas when calculating the percentage of total PDAC area.

To quantify KPC tumor sections, three regions of interest (20× magnification) were randomly selected within the PDAC-positive area as defined by H&E staining of consecutive slides. $CD8^+$ T cell numbers and Sirius Red-stained area were quantified by ImagePro.

For the human TMA, high p53 tumors were defined as those showing intense p53 staining in more than 15% of the cancer cells. $CD8^+$ T cells were quantified in six digital images per tumor, taken at a magnification of 40× using the CaseViewer 3D Histech software; only images containing both cancer cells and surrounding stroma were included. When necessary, a correction for distortion artifact was performed. In each image, $CD8^+$ cells were defined as either proximal (residing within epithelial cell clusters or less than 10 μm from the nearest cancer cell) or distal (residing more than 10 μm from the nearest cancer cell). The number of $CD8^+$ T cells within epithelial cancer cell clusters in each image was normalized to the percentage of the image area covered by cancer cells. Similarly, numbers of $CD8^+$ cells within the stroma were normalized to percentage area composed of stroma. Values from all six images were then combined to calculate the average proximal/distal ratio for each tumor in the TMA.

SHG Imaging. TMAs slides were imaged using an upright Leica TCS SP8 MP microscope, equipped with external non-descanned detectors (NDDs) HyD and Acusto Optical Tunable Filter (Leica-Microsystems CMS, GmbH) and internal HyD detectors for confocal imaging. SHG signal was excited by a tunable femtosecond laser 680 to 1,080 Coherent vision II (Coherent) set to a wavelength of 885 nm at 4% power. Emission signal was collected using an external NDD HyD detector through a long pass filter of 440 nm. Transmitted signal was collected using a photomultiplier (PMT) detector in transmission position. Images were acquired using the galvometric scanner (400 Hz) in a format of 1,024 × 1,024 (XY) with a HC FLUOTAR L 25×/0.95 water objective, pixel size of 0.433 μm XY. Four Z slices were collected per TMA and nine tiles in 10% overlap.

The PA242e TMA set was imaged in sequential mode, imaging tissue SHG, and then confocal microscopy for fluorescent stains using internal HyD detectors was used.

- CD8 excitation: 488 nm (power 0.5%); emission: 494 to 544 nm
- p53 excitation: 566 nm (power 0.5%); emission: 570 to 627 nm
- CK8 excitation: 633 nm (power 0.12%); emission: 644 to 714 nm
- SHG as described above.

The acquired images were visualized using LASX software (Leica Application Suite X, Leica Microsystems CMS, GmbH). The images in this paper were acquired at the Advanced Optical Imaging Unit, the de Picciotto Cancer Cell Observatory in Memory of Wolfgang and Ruth Lesser, Weizmann Institute of Science.

Semiautomatic SHG Image Analysis. We employed a semiautomatic image analysis pipeline. First, we manually outlined four to eight representative neoplastic ducts per patient in all TMAs. The following steps were implemented in Fiji (59) macro: A 10-μm band around each tumor duct was created and max projection of Z-stacks was used. Overlapping band regions and regions at the edges of the TMA were discarded. To identify positive collagen signals, a fixed threshold for each set of TMAs was used. The threshold was selected so that it is higher than the background signal within tumor

regions (which do not contain collagen). To compute the SHG signal score, we determined the fraction area of positive collagen signal within each band and averaged the scores from all bands in the same TMA.

Statistical Data Analysis. Statistical analysis was performed using GraphPad Prism 7.0 software. Mean ± SEM is presented. Survival analysis was done in R, v. 4.0.3, using the package "survival."

Data Availability. All study data are included in the article and/or supporting information.

ACKNOWLEDGMENTS. We thank Yael Aylon, Anat Gershoni, Varda Rotter, Ruth Scherz-Shouval, David Kelsen, David Tuveson, members of the Tuveson laboratory and Calanit Raanan for sharing reagents and for inspiring scientific discussions. This work was supported in part by grants from the Thompson Family Foundation (to M.O.), the Dr. Miriam and Sheldon G. Adelson Medical Research Foundation (to M.O. and M.L.), a grant from Anat and Amnon Shashua, and the Moross Integrated Cancer Center. M.O. is incumbent of the André Lwoff Chair in Molecular Biology. Imaging was made possible thanks to the de Picciotto Cancer Cell Observatory in memory of Wolfgang and Ruth Lesser. M.M. is a recipient of a fellowship from the Sergio Lombroso Program.

1. M. Eileen *et al*., Durvalumab with or without tremelimumab for patients with metastatic pancreatic ductal adenocarcinoma a phase 2 randomized clinical trial. *JAMA Oncol.* **5**, 1431–1438 (2019).
2. Y. Zhu *et al*., CSF1/CSF1R blockade reprograms tumor-infiltrating macrophages and improves response to T-cell checkpoint immunotherapy in pancreatic cancer models. *Cancer Res.* **74**, 5057–5069 (2014).
3. P. Goedegebuure *et al*., Myeloid-derived suppressor cells: General characteristics and relevance to clinical management of pancreatic cancer. *Curr. Cancer Drug Targets* **11**, 734–751 (2011).
4. H. Laklai *et al*., Genotype tunes pancreatic ductal adenocarcinoma tissue tension to induce matricellular-fibrosis and tumor progression. *Nat. Med.* **22**, 497–505 (2016).
5. C. Feig *et al*., Targeting CXCL12 from FAP-expressing carcinoma- associated fibroblasts synergizes with anti–PD-L1 immunotherapy in pancreatic cancer. *Proc. Natl. Acad. Sci. U.S.A.* **110**, 20212–20217 (2013).
6. G. Manley, Activated pancreatic stellate cells sequester CD8+ T-cells to reduce their infiltration of the juxtatumoral compartment of pancreatic ductal adenocarcinoma. *Gastroenterology* **71**, 233–236 (2013).
7. K. P. Olive *et al*., Inhibition of hedgehog signaling enhances delivery of chemotherapy in a mouse model of pancreatic cancer. *Science* **324**, 1457–1461 (2009).
8. Y. Ino *et al*., Immune cell infiltration as an indicator of the immune microenvironment of pancreatic cancer. *Br. J. Cancer* **108**, 914–923 (2013).
9. C. E. Clark *et al*., Dynamics of the immune reaction to pancreatic cancer from inception to invasion. *Cancer Res.* **67**, 9518–9527 (2007).
10. Y. Posen *et al*., Manipulation of redox signaling in mammalian cells enabled by controlled photogeneration of reactive oxygen species. *J. Cell Sci.* **118**, 1957–1969 (2005).
11. D. von Ahrens, T. D. Bhagat, D. Nagrath, A. Maitra, A. Verma, The role of stromal cancer-associated fibroblasts in pancreatic cancer. *J. Hematol. Oncol.* **10**, 10–76 (2017).
12. D. Öhlund *et al*., Distinct populations of inflammatory fibroblasts and myofibroblasts in pancreatic cancer. *J. Exp. Med.* **214**, 579–596 (2017).
13. K. Y. Elahi-Gedwillo, M. Carlson, J. Zettervall, P. P. Provenzano, Antifibrotic therapy disrupts stromal barriers and modulates the immune landscape in pancreatic ductal adenocarcinoma. *Cancer Res.* **79**, 372–386 (2019).
14. H. Jiang *et al*., Targeting focal adhesion kinase renders pancreatic cancers responsive to checkpoint immunotherapy. *Nat. Med.* **22**, 851–860 (2017).
15. A. J. Levine, p53: 800 million years of evolution and 40 years of discovery. *Nat. Rev. Cancer* **20**, 471–480 (2020).
16. P. A. J. Muller, K. H. Vousden, Mutant p53 in cancer: New functions and therapeutic opportunities. *Cancer Cell* **25**, 304–317 (2014).
17. M. Oren, V. Rotter, Mutant p53 gain-of-function in cancer. *Cold Spring Harb. Perspect. Biol.* **2**, a001107 (2010).
18. B. J. Raphael *et al*.; Cancer Genome Atlas Research Network, Integrated genomic characterization of pancreatic ductal adenocarcinoma. *Cancer Cell* **32**, 185–203.e13 (2017).
19. S. M. Wörmann *et al*., Loss of P53 function activates JAK2-STAT3 signaling to promote pancreatic tumor growth, stroma modification, and gemcitabine resistance in mice and is associated withpatient survival. *Gastroenterology* **151**, 180–193 (2016).
20. I. Amelio *et al*., p53 mutants cooperate with HIF-1 in transcriptional regulation of extracellular matrix components to promote tumor progression. *Proc. Natl. Acad. Sci. U.S.A.* **115**, E10869–E10878 (2018).
21. V. Capaci *et al*., Mutant p53 induces Golgi tubulo-vesiculation driving a prometastatic secretome. *Nat. Commun.* **11**, 3945 (2020).
22. C. Vennin *et al*.; Australian Pancreatic Genome Initiative (APGI), CAF hierarchy driven by pancreatic cancer cell p53-status creates a pro-metastatic and chemoresistant environment via perlecan. *Nat. Commun.* **10**, 3637 (2019).
23. J. Blagih, M. D. Buck, K. H. Vousden, P53, cancer and the immune response. *J. Cell Sci.* **133**, jcs.237453 (2020).
24. G. Yang *et al*., Senescence and tumour clearance is triggered by p53 restoration in murine liver carcinomas. *Nature* **344**, 1173–1178 (2017).
25. A. Iannello, T. W. Thompson, M. Ardolino, S. W. Lowe, D. H. Raulet, p53-dependent chemokine production by senescent tumor cells supports NKG2D-dependent tumor elimination by natural killer cells. *J. Exp. Med.* **210**, 2057–2069 (2013).
26. T. Cooks *et al*., Mutant p53 cancers reprogram macrophages to tumor supporting macrophages via exosomal miR-1246. *Nat. Commun.* **9**, 771 (2018).
27. J. Blagih *et al*., Cancer-specific loss of p53 leads to a modulation of myeloid and T cell responses. *Cell Rep.* **30**, 481–496 (2020).
28. Z. Jiang, Z. Liu, M. Li, C. Chen, X. Wang, Immunogenomics analysis reveals that TP53 mutations inhibit tumor immunity in gastric cancer. *Transl. Oncol.* **11**, 1171–1187 (2018).
29. M. D. Wellenstein *et al*., Loss of p53 triggers WNT-dependent systemic inflammation to drive breast cancer metastasis. *Nature* **572**, 538–542 (2019).
30. I. Peran, S. Madhavan, S. W. Byers, M. D. McCoy, Curation of the pancreatic ductal adenocarcinoma subset of the cancer genome atlas is essential for accurate conclusions about survival-related molecular mechanisms. *Clin. Cancer Res.* **24**, 3813–3819 (2018).
31. J. Galon, D. Bruni, Approaches to treat immune hot, altered and cold tumours with combination immunotherapies. *Nat. Rev. Drug Discov.* **18**, 197–218 (2019).
32. E. S. Knudsen *et al*., Stratification of pancreatic ductal adenocarcinoma: Combinatorial genetic, stromal, and immunologic markers. *Clin. Cancer Res.* **23**, 4429–4440 (2017).
33. V. Thorsson *et al*.; Cancer Genome Atlas Research Network, The immune landscape of cancer. *Immunity* **48**, 812–830 (2018).
34. S. V. Puram *et al*., Single-cell transcriptomic analysis of primary and metastatic tumor ecosystems in head and neck cancer. *Cell* **171**, 1611–1624 (2017).
35. S. R. Hingorani *et al*., Trp53R172H and KrasG12D cooperate to promote chromosomal instability and widely metastatic pancreatic ductal adenocarcinoma in mice. *Cancer Cell* **7**, 469–483 (2005).
36. J. Reimand, M. Kull, H. Peterson, J. Hansen, J. Vilo, g:Profiler–A web-based toolset for functional profiling of gene lists from large-scale experiments. *Nucleic Acids Res.* **35**, W193–W200 (2007).
37. D. R. Principe *et al*., TGFβ signaling in the pancreatic tumor microenvironment promotes fibrosis and immune evasion to facilitate tumorigenesis. *Cancer Res.* **76**, 2525–2539 (2016).
38. H. Salmon *et al*., Matrix architecture defines the preferential localization and migration of T cells into the stroma of human lung tumors. *J. Clin. Invest.* **122**, 899–910 (2012).
39. C. Tian *et al*., Proteomic analyses of ECM during pancreatic ductal adenocarcinoma progression reveal different contributions by tumor and stromal cells. *Proc. Natl. Acad. Sci. U.S.A.* **116**, 19609–19618 (2019).
40. D. Thomas, P. Radhakrishnan, Tumor-stromal crosstalk in pancreatic cancer and tissue fibrosis. *Mol. Cancer* **18**, 14 (2019).
41. B. Piersma, M. K. Hayward, V. M. Weaver, Fibrosis and cancer: A strained relationship. *Biochim. Biophys. Acta Rev. Cancer* **1873**, 188356 (2020).
42. A. Neesse *et al*., Stromal biology and therapy in pancreatic cancer: Ready for clinical translation? *Gut* **68**, 159–171 (2019).
43. M. W. L. Teng, S. F. Ngiow, A. Ribas, M. J. Smyth, Classifying cancers based on T cell infiltration and PD-L1. *Cancer Res.* **75**, 2139–2145 (2017).
44. M. Hilmi, L. Bartholin, C. Neuzillet, Immune therapies in pancreatic ductal adenocarcinoma: Where are we now? *World J. Gastroenterol.* **24**, 2137–2151 (2018).
45. J. L. Carstens *et al*., Depletion of carcinoma-associated fibroblasts and fibrosis induces immunosuppression and accelerates pancreas cancer with reduced survival. *Cancer Cell* **25**, 719–734 (2008).
46. D. V. T. Catenacci *et al*., Randomized phase Ib/II study of gemcitabine plus placebo or vismodegib, a hedgehog pathway inhibitor, in patients with metastatic pancreatic cancer. *J. Clin. Oncol.* **33**, 4284–4292 (2015).
47. A. D. Rhim *et al*., Stromal elements act to restrain, rather than support, pancreatic ductal adenocarcinoma. *Cancer Cell* **25**, 735–747 (2015).
48. E. Kotler *et al*., A systematic p53 mutation library links differential functional impact to cancer mutation pattern and evolutionary conservation. *Mol. Cell* **71**, 178–190 (2018).
49. A. O. Giacomelli *et al*., Mutational processes shape the landscape of TP53 mutations in human cancer. *Nat. Genet.* **50**, 1381–1387 (2018).
50. S. Boettcher *et al*., A dominant-negative effect drives selection of TP53 missense mutations in myeloid malignancies. *Science* **365**, 599–604 (2020).
51. S. Weissmueller *et al*., Mutant p53 drives pancreatic cancer metastasis through cell-autonomous PDGF receptor β signaling. *Cell* **157**, 382–394 (2014).
52. S. Arandkar *et al*., Altered p53 functionality in cancer-associated fibroblasts contributes to their cancer-supporting features. *Proc. Natl. Acad. Sci. U.S.A.* **115**, 6410–6415 (2018).
53. A. Hoshino *et al*., Extracellular vesicle and particle biomarkers define multiple human cancers. *Cell* **182**, 1044–1061 (2020).
54. Y. Addadi *et al*., p53 status in stromal fibroblasts modulates tumor growth in an SDF1-dependent manner. *Cancer Res.* **70**, 9650–9658 (2010).
55. A. Chakravarthy, L. Khan, N. P. Bensler, P. Bose, D. D. De Carvalho, TGF-β-associated extracellular matrix genes link cancer-associated fibroblasts to immune evasion and immunotherapy failure. *Nat. Commun.* **9**, 4692 (2018).
56. M. Ghosh *et al*., Mutant p53 suppresses innate immune signaling to promote tumorigenesis. *Cancer Cell* **39**, 494–508 (2021).
57. H. Ahn *et al*., (2017) Improving survival by exploiting tumor dependence on stabilized mutant p53 for treatment. *Physiol. Behav.* **176**, 139–148 (2017).
58. K. P. Olive, D. A. Tuveson, The use of targeted mouse models for preclinical testing of novel cancer therapeutics. *Clin. Cancer Res.* **12**, 5277–5287 (2006).
59. J. Schindelin *et al*., Fiji: An open-source platform for biological-image analysis. *Nat. Methods* **9**, 676–682 (2012).